Real-time emulation of a MMC with BESS for EV application

Alaa Omar
Department of Electrical and Computer
Engineering
University of Canterbury
Christchurch, NEW ZEALAND
alaa.omar@pg.canterbury.ac.nz

Alan Wood
Department of Electrical and Computer
Engineering
University of Canterbury
Christchurch, NEW ZEALAND
alan.wood@canterbury.ac.nz

Hamish Laird
Department of Electrical and Computer
Engineering
University of Canterbury
Christchurch, NEW ZEALAND
hamish.laird@elmgdigitalpower.com

Paul Gaynor
Department of Electrical and Computer
Engineering
University of Canterbury
Christchurch, NEW ZEALAND
paul.gaynor@canterbury.ac.nz

Abstract— A real-time emulation of a modular multilevel converter with integrated energy storage devices has been carried out. The real-time model is detailed and implemented using MicroLabBox/dSPACE. The system is tested and compared to an experimental prototype of the converter. The main advantage of the proposed real-time system is that it gives higher fidelity for further investigations, specifically in electric vehicle applications where it can be integrated into a real-time emulated electric vehicle. The model can be extended to a higher number of levels as it has no constraints on the number of switches or batteries/cells. Also, it can be integrated in a power hardware in the loop system to decrease the testing time of a product. This is a novel proposal of a real-time emulation of the converter in an electric vehicle application using MicroLabBox/dSPACE.

Keywords—real-time, emulation, MMC, batteries, HIL.

I. INTRODUCTION

The dynamic performance of electrical systems can be tested using various simulation tools. Dynamic simulation is very helpful in the early stages of the design phase during a product development cycle. However, the testing fidelity of simulation platforms is low as shown in Fig. 1 [1]. Hardware in the loop (HIL) testing methods have higher fidelity than simulation tools [2]. HIL testing can be classified into the controller hardware in the loop (CHIL) and power hardware in the loop (PHIL). When a controller is interfaced to an emulation platform that can process the dynamics of a specific system in real-time, the HIL testing arrangement is called CHIL. The PHIL methodology indicates that the emulation platform is interfaced to physical components as part of the complete system. As an example, the HIL is used to interface an amplifier to generate a higher magnitude AC waveform to test the response of an electric motor. The speed feedback of the motor is measured and is used as an input to the HIL. In that case, the HIL platform is used as the inverter.

The main advantage of the HIL platforms is the real-time implementation of the system dynamics. This feature enables the integration of the HIL devices into the prototype system. Commercial HIL platforms such as Typhoon HIL, dSPACE, and Speedgoat offer many products that can be utilized as a HIL platform. A customized library is used to build the system using pre-configured blocks of the system devices. When emulating the systems that comprise a large number of switches or batteries/cells, some limitation confines the range of the emulated systems. An example, Typhoon HIL has a limit of 8 batteries (based on lookup tables) that can be concurrently emulated in one HIL604. To increase the number of available devices, up to 16 platforms can be connected to a unified HIL system via a single link. In a modular multilevel converter with battery energy storage devices (MMC-BESS), more than a hundred batteries are expected to be embedded in one arm. This adds a burden on the real-time processor and might lead to task overrun.

In this research, a *MicroLabBox/dSPACE* is used to emulate a real-time operation of an MMC-BESS. *MicroLabBox* is typically used as a rapid prototyping controller for fast implementation of control systems using Simulink/Matlab interface. However, no dedicated physical library blocks (switches or batteries) are available to implement the real-time prototypes of the converter using *MicroLabBox*. Thus, the converter dynamic equations are used to emulate the converter performance in real-time. There is no limit on the number of batteries. Switches are ideally represented to facilitate the extension of the converter to a large number of levels without task overrun nor significantly decreasing the sampling time. This work presents a complete dynamic model of the MMC, which can be connected to any load as CHIL or PHIL with high fidelity. The real-time emulated converter is compared to a prototype of the converter. The system can be extended to include emulated EVs. This model representation can be used for model predictive control of the MMC-BESS.
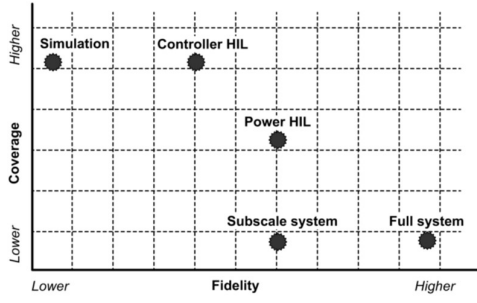
Fig. 1. Comparison between power testbed types [1].

II. MMC MODEL DETAILS

A. Battery modeling

There are various approaches to model battery dynamics. While the complex representation of the battery depends on a detailed physical model of the battery dynamics, other methods utilize simple modelling of the battery voltage and current. The look-up table method proposed in [3], also used by PLECS software to simulate a Lithium-Ion cell [4], is an effective method that utilizes the battery discharge curves to implement the battery model. In the look-up method, the battery discharge curve at the nominal discharge rate (1C) is used to emulate a battery operation.

Assuming that the battery temperature (T) is constant and the battery terminal voltage and state of discharge $(v_t - SOD)$ curve is given at the rated discharge rate; the open circuit voltage can be calculated using battery internal resistance. Battery internal resistance is given in the battery datasheet. If not given, it can be calculated from the terminal voltage difference (Δv_t) at two different discharge rates $(i_{t\_rated}, and\ i_{t\_2})$ when SOD=0 [3]. The battery internal resistance equals

$$R_{int} = \frac{\Delta v_t}{i_{t\_rated} - i_{t\_2}} \tag{1}$$

Open circuit voltage at the rated discharge rate can be calculated from the equation

$$v_{oc} = v_t + R_{int} i_{t\_rated} \tag{2}$$

Once the battery relation $v_{oc} - SOC$ is defined and the battery initial state of charge (SOC) is known, Coulomb counting SOC estimation can be utilised to calculate the battery SOC variations from the relation

$$SOC(t) = SOC(t_i) - \frac{\eta_{bat}}{3600 * Q_{max}} \int_{t_i}^{t} i(t)\, dt \tag{3}$$

where $\eta_{bat}(T, i(t))$ is the coulombic efficiency of the battery and $Q_{max}(T)$ is the battery maximum capacity in ampere-seconds.

A detailed battery model based on the look-up table method is shown in Fig. 2. The battery v_{oc} is calculated via the $v_{oc} - SOC$ look-up table. The next step is to calculate battery terminal voltage by substitution in equation (2). For accurate battery modelling, linear correction factors can be used to consider the temperature and discharge rate effects on the battery dynamic voltage [3]. Dynamic voltage variations in a battery can be expressed in terms of v_{oc}, the battery state of charge SOC and battery temperature T as [3, 4]

$$v_{oc} + v_d = SOC\ (i, T) + \Delta E(T) = k_1[i(t)].k_2[T(t)] + \Delta E(T) \tag{4}$$

where $SOC\ (i, T)$ is dependent on the discharge current and temperature. $\Delta E(T)$, is a correction voltage that is added to v_{oc} to represent the changes in the battery temperature with time. k_1 is the first correction factor that is dependent on the discharge rate. k_2 is the correction factor that describes the temperature effect on the battery SOC [4].

The implementation of the correction values is shown in Fig. 2. The challenge of the battery model is to determine the correction factors at different discharge rates and at different temperature values. Temperatures below 0° C degrade the battery performance and increase the battery internal resistance [5]. Terminal voltage decreases proportionally with the temperature decrease. At higher temperature values, the voltage will increase, but the high temperature accelerates the ageing of Lithium ion batteries and may lead to irreversible changes of the battery chemistry.

Lijun et al. [3] proposed a lookup table method to determine the temperature and discharge correction factors from given battery discharge curves. This method gives an approximation of the battery performance during different discharge rates. Practically, the temperature during discharge rises and is dependent on the discharge rate itself.
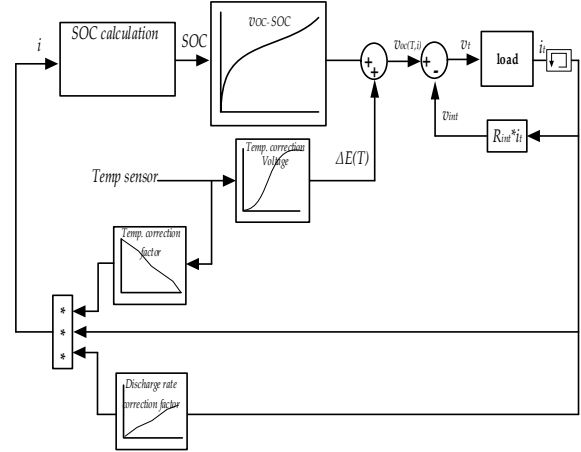

Fig. 2. Battery model blocks based on lookup table method.

Lithium-Ion cell INR18650-25R, made by Samsung, has discharge curves at 1C, 2C, 4C, and 6C, shown in Fig. 3. The cell model is simulated at the same discharge rates of the given manufacturer data. Cell temperature has been increased using multidimensional look-up table to emulate the actual temperature rise at higher discharge rates as given by the manufacturer. As shown in Fig. 3, discharge curves that have been obtained by the battery model in this research are very close to the actual manufacturer curves. Being part of the basic structure of the MMC-BESS, the battery model gives high fidelity results for the MMC operation. In the following real-time emulation results, the temperature and the voltage correction factors are assumed constant.
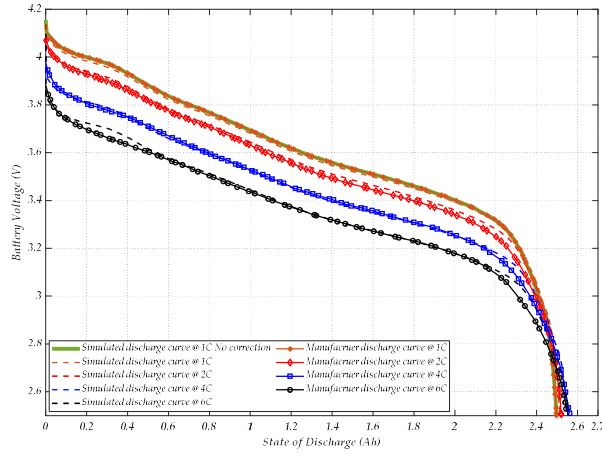
Fig. 3. Battery discharge curves at 1C, 2C, 4C, and 6C.

B. Arm modeling

The inverter arm consists of a series of submodules (SMs) which comprise batteries and switches. The battery model is already detailed in subsection A. The SM switches can be modelled with a detailed representation of nonlinear elements (driver circuit or switch dynamics)[6]. For an increased number of levels, this modelling approach requires a significant modelling time to handle the large number of nodal analyses. In a simpler representation, conduction losses of the switch can be described by on-resistance in milliohms; the off state can be represented by a high resistance [7]. Further simplification can be implemented by representing the arm equivalent model. However, this is only applicable for power system analysis, as there is no access to the individual SM dynamic variables. In this research, the SM is represented by its state variables during ON and OFF state as described below.

1) SM representation

The SM can be modelled using the battery state variables according to its switching status as shown in Fig. 4 and listed in TABLE I. Based on the state variable representation, a SM can be modelled as a voltage source. The SM output voltage equals the battery terminal voltage when inserted. When the SM is bypassed, its output voltage equals zero. As the switches in a SM are complementary, only one switch is used to represent the two switches. The auxiliary switch s_x status represents a SM inserted when $s_x = 1$ or ON. A SM is bypassed when $s_x = 0$ or OFF. This representation is used to determine the output voltage of a SM. If the auxiliary switch is ON, then the output voltage of the SM is the battery voltage, else the output voltage is zero. The battery current equals the arm current when the battery is inserted as the arm current flows through the battery. When bypassed, the battery current equals zero. Of note here is that the blocked status (both switched are off) is not represented. The design of the prototype switch gate drive follows the same representation, i.e. one switch is always on.
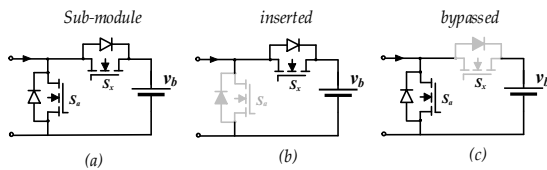

Fig. 4. Submodule switching status.

TABLE I. THE STATE VARIABLES OF A SUBMODULE

S_x	S_a	State variables
1	0	$v_{SM} = v_{battery}$ $i_{battery} = i_{arm}$
0	1	$v_{SM} = 0$ $i_{battery} = 0$ $v_{battery} = unchanged$

2) Arm representation

Assuming N submodules per arm, the switching vector in one arm is $sw_v = [s_{x,1}, s_{x,2}, \ldots .. s_{x,n}]$. The insertion index can be used to calculate the voltage of the switched on SMs in one arm (NV_c) as

$$v_{xu,l} = \sum_{i=1}^{i=n} s_{x,i} v_{bat,i} \text{ where } s_{x,i} \in \{0,1\} \quad (5)$$

Maximum insertion indices (i_{max}) equals the total number of the SMs (N). Equivalent arm ON resistance R_{on_arm} of the active SMs can be subtracted from the arm voltage in equation (5) as

$$v_{xu} = \sum_{i=1}^{i=n} (s_{x,i} v_{bat,i} - i_{arm} R_{on,i}) \quad (6)$$

Including large number of look-up tables up to many hundreds in one arm, dramatically overload the processor to emulate the real-time performance of the converter. Thus, only one look-up table per arm is used, and the batteries are modeled as a voltage vector.

C. Complete dynamic model of the converter

The dynamic model of the MMC-BESS converter can be driven similar to the representation that has been presented by Dekka et al in [8] to detail the dynamic model of the conventional MMC. The main difference is that the detailed battery model replaces the capacitor. Also, there is no current that flows in a DC link capacitor between the upper and the lower bus bars (that is, there isno DC link), as shown in Fig. 5. Assuming that the DC current that flows in the DC virtual bus bar is divided into three equal parts in the three legs, the arm current can be written in a form of the DC current, phase current and the circulating current as follows

$$\left. \begin{array}{l} i_{au} = \frac{i_{dc}}{3} + i_{cir,a} + \frac{i_a}{2} \, , i_{al} = \frac{i_{dc}}{3} + i_{cir,a} - \frac{i_a}{2} \\ i_{bu} = \frac{i_{dc}}{3} + i_{cir,b} + \frac{i_b}{2} \, , i_{bl} = \frac{i_{dc}}{3} + i_{cir,b} - \frac{i_b}{2} \\ i_{cu} = \frac{i_{dc}}{3} + i_{cir,c} + \frac{i_c}{2} \, , i_{cl} = \frac{i_{dc}}{3} + i_{ci\ ,c} - \frac{i_c}{2} \end{array} \right\} \quad (8)$$
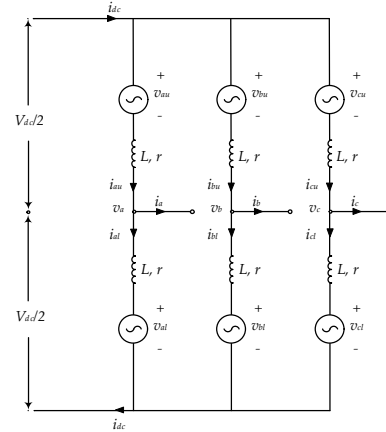

Fig. 5. Equivalent circuit of a three phase MMC-BESS.

By adding the three phases currents in equation (8) together, the DC current equals

$$i_{dc} = \sum_{x=a,b,c} i_{xu} = \sum_{x=a,b,c} i_{xl} = \frac{1}{2}\sum_{x=a,b,c} i_{xu} + i_{xl} \quad (9)$$

The DC current that flows in the positive and the negative bus bars of the converter is the total current in the upper or the lower arms of the converter.

As shown in Fig. 5, the upper and the lower arm voltages ($v_{u,x}$ and $v_{l,x}$) of any phase x can be expressed as

$$\left.\begin{array}{l} v_{xu} = \frac{V_{dc}}{2} - v_x - L\frac{di_{xu}}{dt} - ri_{xu} \\ v_{xl} = \frac{V_{dc}}{2} + v_x - L\frac{di_{xl}}{dt} - ri_{xl} \end{array}\right\} \quad (10)$$

The DC voltage can be expressed by adding the upper and the lower voltage equations as

$$V_{dc} = v_{xu} + v_{xl} + L\frac{d(i_{xu}+i_{xl})}{dt} + r(i_{xu} + i_{xl}) \quad (11)$$

Arm currents can be written in terms of the circulating current $i_{cir,x}$ and phase current i_x as

$$\left.\begin{array}{l} i_{xu} = i_{cir,x} + \frac{i_x}{2} \\ i_{xl} = i_{cir,x} - \frac{i_x}{2} \end{array}\right\}, i_{cir,x} = \frac{i_{u,x}+i_{l,x}}{2} \quad (12)$$

A dynamic model of the DC bus current can be driven from the DC voltage equations of each phase. Based on equation 11, the DC voltage of phases A, B, and C equals

$$\left.\begin{array}{l} V_{dc,a} = v_{au} + v_{al} + L\frac{d(i_{au}+i_{al})}{dt} + r(i_{au} + i_{al}) \\ V_{dc,b} = v_{bu} + v_{bl} + L\frac{d(i_{bu}+i_{bl})}{dt} + r(i_{bu} + i_{bl}) \\ V_{dc,c} = v_{cu} + v_{cl} + L\frac{d(i_{cu}+i_{cl})}{dt} + r(i_{cu} + i_{cl}) \end{array}\right\} \quad (13)$$

The instantaneous average DC voltage can be calculated by adding the DC voltage in the three phases and substituting with the DC current value in equation (9) as

$$3V_{dc} = v_{au} + v_{al} + v_{bu} + v_{bl} + v_{cu} + v_{cl} + 2L\frac{di_{dc}}{dt} + 2ri_{dc} \quad (14)$$

By solving equation 14, the dynamic DC current equals

$$\frac{di_{dc}}{dt} = \frac{1}{2L}\left[3V_{dc} - \sum_{x=a,b,c}(v_{xu} + v_{xl}) - 2ri_{dc}\right] \quad (15)$$

To get the dynamic equation which describes the circulating current in any phase x in terms of the arm voltages and the DC voltage, the upper and the lower arm currents in equation 11 will be replaced by the circulating current equation in equation 12 as

$$V_{dc} = v_{xu} + v_{xl} + 2L\frac{d(i_{cir,x})}{dt} + 2r(i_{cir,x}) \quad (16)$$

By solving equation 16, for the circulating current in phase A and by substituting the V_{dc} in phase A, the dynamic circulating current can be written as

$$\frac{di_{cir,a}}{dt} = \frac{1}{6L}\left[\sum_{x=a,b,c}(v_{xu} + v_{xl}) - 3(v_{au} + v_{al}) - 6ri_{cir,a}\right] \quad (17)$$

Similarly, dynamic circulating current in phase B and C can be represented.

III. COMPARISON OF THE PROTOTYPE AND THE HIL PERFORMANCE

The converter prototype is connected to a three phase RL load as shown in Fig. 6. TABLE II details the main converter parameters. The converter is tested utilizing two modulation techniques, Nearest Level Control (NLC) and Phase Shifted PWM (PSPWM). The sorting algorithm proposed in [9] is used to test the balancing of the batteries SOC inside one arm. No arm or leg balancing control is implemented in this study. The *MicroLabBox* is used to emulate the real-time operation of the converter.
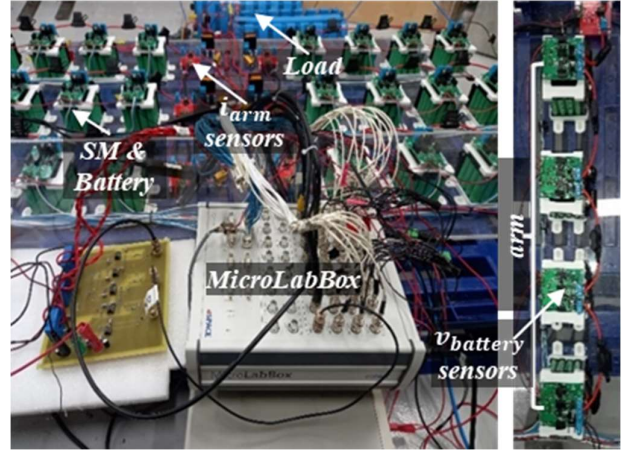

Fig. 6. Experimental setup.

TABLE II. EXPERIMENTAL SETUP PARAMETERS

Variable	Value
SM battery	INR18650-25R
Nominal Battery voltage	7.4 V
L@2kHz	41.2 µH
r@2kHz	0.068 Ω
Ro	5 Ω
Lo	5.32 mH

1) Using NLC modulation

The converter duty ratio is set at 0.8. At the start of operation, the batteries SOC is unbalanced. The NLC is modulated at 50 Hz, the arm resistance r is 0.025 Ω at 50 Hz. Thus, an additional arm resistor of 0.6 Ω is inserted in each arm to limit the high current during the NLC operation. During normal operation while the SMs SOC are nearly equalized, there is no need for the additional resistor. Fig. 7(a), Fig. 8(a), and Fig. 9(a) show experimental waveforms of arm currents and voltages in the three phases of the converter, respectively. The corresponding real-time emulated waveforms are shown in Fig. 7(b), Fig. 8(b), and Fig. 9(b), respectively. Phase current in phases A, B, and C are shown in Fig. 10. The duty ratio is changed from 0.8 to 0.9 in Fig. 7(a), and Fig. 7(b) to show the dynamic change in both the prototype and the real-time emulated systems. The sampling time for the prototype and the emulated system is 40 µs.
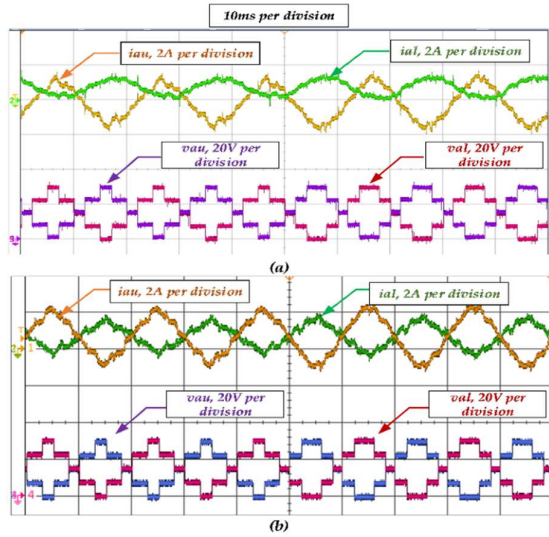
Fig. 7. The upper and the lower arm currents and voltages in phase A during NLC: (a) prototype converter, (b) real-time HIL.
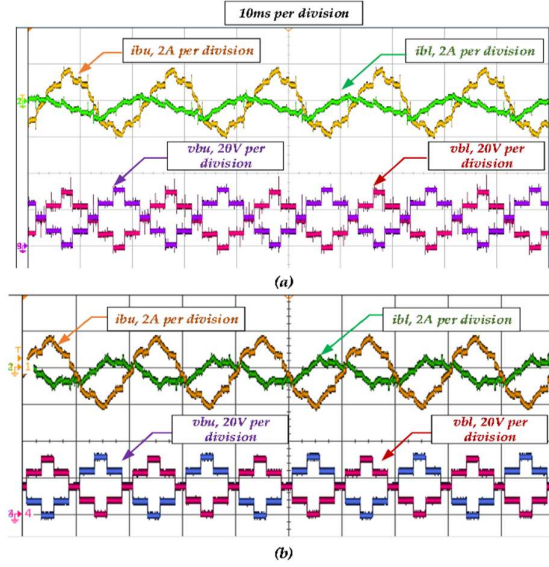

Fig. 8. The upper and the lower arm currents and voltages in phase B during NLC: (a) prototype converter, (b) real-time HIL.
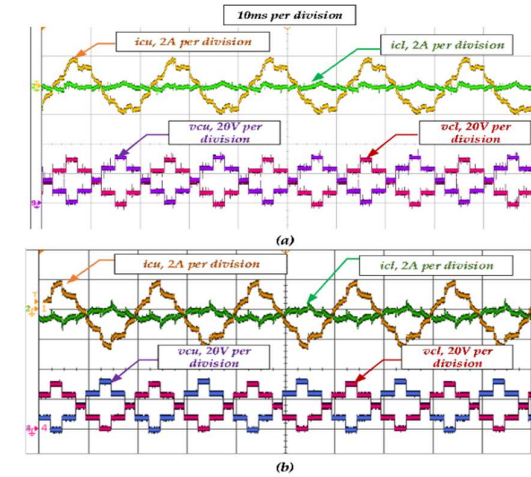

Fig. 9. The upper and the lower arm currents and voltages in phase C during NLC: (a) prototype converter, (b) real-time HIL.

2) Using PSPWM modulation

NLC is a simple and effective modulation strategy when used to switch large number of levels [9]. However, its performance is highly disturbed at low levels as shown in Fig. 10 (a) and (b). PSPWM is used as the modulation strategy and the corresponding phase currents are shown in Fig. 10 (C). PSPWM is used at 2 kHz which makes the effective arm resistance equals 0.064. The additional arm resistor 0.6 Ω is removed. The converter operation is tested for 3400 seconds. The current and voltage waveforms during experimental operation and real-time emulation are shown in Fig. 11, Fig. 12, and Fig. 13, respectively.
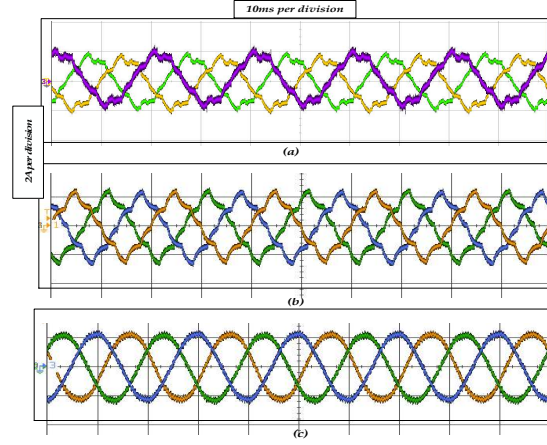

Fig. 10. Phase currents : (a) prototype converter (NLC), (b) real-time HIL (NLC), and (c) real-time HIL (PSPWM).
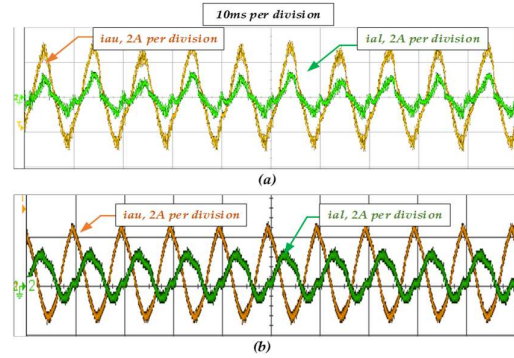

Fig. 11. The upper and the lower arm currents and voltages in phase A during PSPWM: (a) prototype converter, (b) real-time HIL.
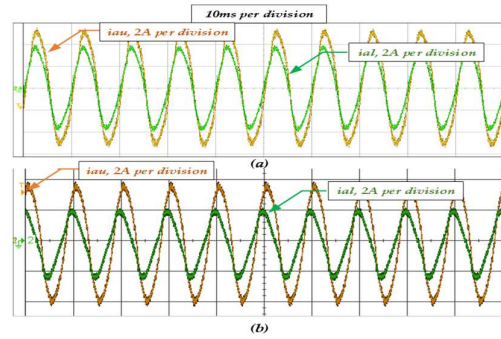

Fig. 12. The upper and the lower arm currents and voltages in phase B during PSPWM: (a) prototype converter, (b) real-time HIL.
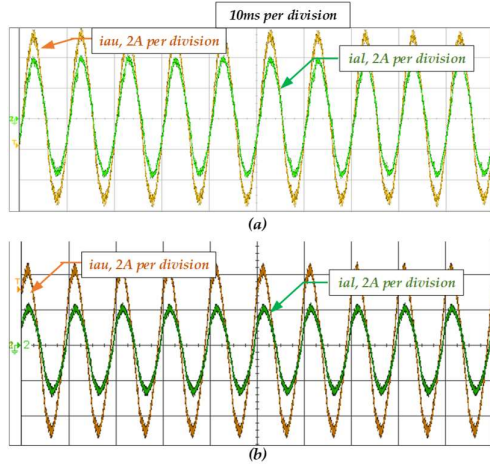
Fig. 13. The upper and the lower arm currents and voltages in phase C during PSPWM: (a) prototype converter, (b) real-time HIL.

Batteries SOC in the converter arms is shown in Fig. 14 for the prototype and in Fig. 15 for the emulated converter. Initial SOC of the batteries is different in the prototype, and the same values are used for the emulated system. There is a slight difference at the end of the operation between the actual and emulated batteries SOC. This is due to reasons which include the current measurement error and arm resistance differences. It is assumed that all arms have the same inductance and resistance, but this is not the typical case. Additional deviation is due to the battery model. While the battery model is proven to be very close to the actual battery, battery terminal voltage and internal resistance is different from one battery to another, in addition to the measurement error of the battery voltage sensor.
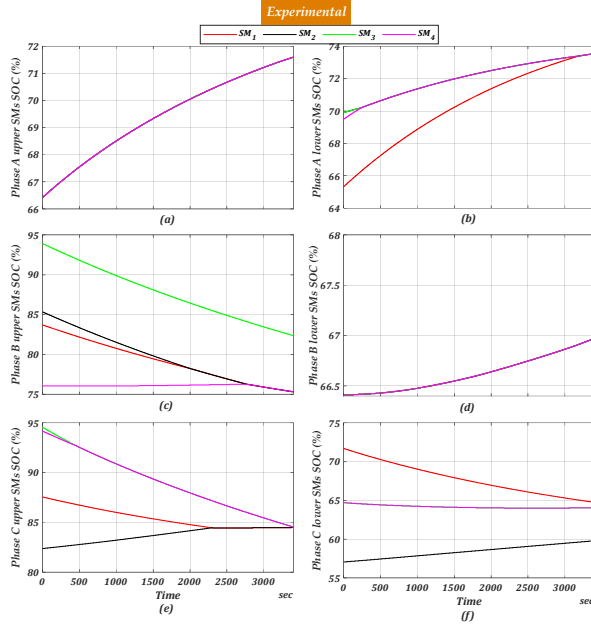

Fig. 14. Individual batteries SOC in the prototype converter: (a) upprer arm A, (b) lower arm A, (c) upper arm B, (d) lower arm B, (e) upper arm C, and (f) lower arm C.
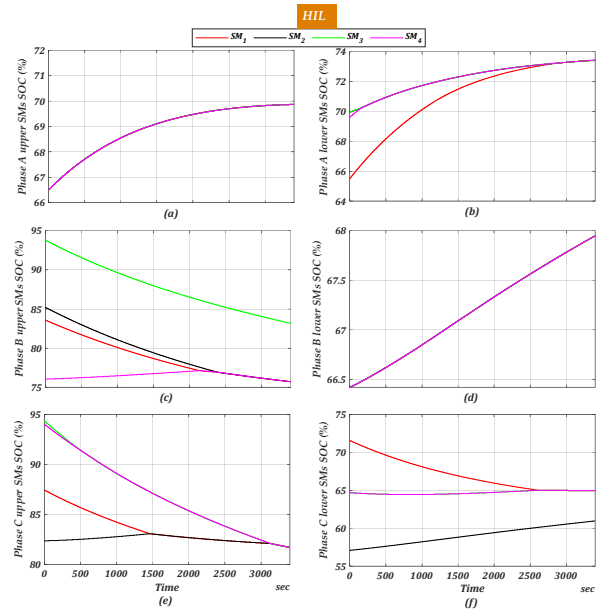

Fig. 15. Individual batteries SOC in the real-time HIL: (a) upprer arm A, (b) lower arm A, (c) upper arm B, (d) lower arm B, (e) upper arm C, and (f) lower arm C.

IV. CONCLUSION

Complete real-time emulation of the MMC-BESS is described in this study. The comparison of the test results in the case of the prototype and the real-time emulation showed that the switching representation is valid and sufficient to model the converter. A novel CHIL of the MMC-BESS is presented using *MicroLabBox.* This CHIL is not limited to a specific number of elements and can be utilized as PHIL for further investigations of EV systems.

V. REFERENCES

[1] "IEEE Standard for the Testing of Microgrid Controllers," *IEEE Std 2030.8-2018,* pp. 1-42, 2018.
[2] H. Magnago, H. Figueira, O. Gagrica, and D. Majstorovic, "HIL-based certification for converter controllers: Advantages, challenges and outlooks (Invited Paper)," in *2021 21st International Symposium on Power Electronics (Ee),* 2021, pp. 1-6.
[3] G. Lijun, L. Shengyi, and R. A. Dougal, "Dynamic lithium-ion battery model for system simulation," *IEEE Transactions on Components and Packaging Technologies,* vol. 25, no. 3, pp. 495-505, 2002.
[4] J. Schonberger, "Modeling a lithium-ion cell using PLECS," *Plexim GmbH,* pp. 1-5, 2009.
[5] S. Ma *et al.*, "Temperature effect and thermal impact in lithium-ion batteries: A review," *Progress in Natural Science: Materials International,* vol. 28, no. 6, pp. 653-666, 2018.
[6] Z. Shen and V. Dinavahi, "Real-Time Device-Level Transient Electrothermal Model for Modular Multilevel Converter on FPGA," *IEEE Transactions on Power Electronics,* vol. 31, no. 9, pp. 6155-6168, 2016.
[7] H. Saad, C. Dufour, J. Mahseredjian, S. Dennetiere, and S. Nguefeu, "Real Time simulation of MMCs using the State- Space Nodal Approach," 2013.
[8] A. Dekka, "High-Power Modular Multilevel Converters: Modeling, Modulation And Control," PhD, Ryerson University, 2017.
[9] A. Omar, A. Wood, H. Laird, and P. Gaynor, "Single-Phase Charging of EV Embedded Batteries in an MMC with Submodule Override Capability," *Energies,* vol. 15, no. 6, p. 2276, 2022.